

Improving Task Adaptation for Cross-domain Few-shot Learning

Wei-Hong Li
 w.h.li@ed.ac.uk
 Xialei Liu
 xliu77@ed.ac.uk
 Hakan Bilen
 hbilien@ed.ac.uk

VICO Group
 University of Edinburgh
 Edinburgh, United Kingdom

Abstract

In this paper, we look at the problem of cross-domain few-shot classification that aims to learn a classifier from previously unseen classes and domains with few labeled samples. We study several strategies including various adapter topologies and operations in terms of their performance and efficiency that can be easily attached to existing methods with different meta-training strategies and adapt them for a given task during meta-test phase. We show that parametric adapters attached to convolutional layers with residual connections performs the best, and significantly improves the performance of the state-of-the-art models in the Meta-Dataset benchmark with minor additional cost. Our code will be available at <https://github.com/VICO-UoE/URL>.

1 Introduction

Few-shot classification [18, 27] is a widely studied problem, where few-shot tasks consist of two sets of samples, *i.e.* *support set* and *query set*. The task is defined by a support set which contains K instances per class sampled over N different classes, known as N -way K -shot, where K can be as small as one. The goal is to label each sample in the query set with the ground truth – one of N classes in support set. Most existing methods [2, 39, 40, 44] use a two-step meta-learning procedure, where a model is learned with a training set in *meta-training* phase and adapted to disjoint classes in *meta-test* phase.

Earlier works made significant progress in homogeneous few-shot tasks, where models are trained and evaluated on samples from a single distribution, such as Ominglot [19], miniImageNet [24] and tieredImageNet [34]. Recently, the field has been shifting towards a more challenging few-shot classification scenario across multiple datasets (or domains) (Meta-Dataset [43]). This multi-domain setting poses two main challenges for the few-shot learning methods. First, as visual characteristics significantly vary across different domains, a successful few-shot method must selectively transfer knowledge from previously seen domains. To this end, previous works learn to adaptively select the *related* domain-specific knowledge based on a given support set via either handcrafted feature selection [10], attention mechanism [24] or producing initialization for the network weights [2]. Second, it has to

efficiently leverage the limited information in the small support set without overfitting to them and adapt to the new task. Prior methods focusing on this challenge involve finetuning the whole model [6, 9], learning a linear classifier [21] and high-dimensional mapping [22]. While the methods addressing the first and second challenges are typically applied either in meta-train or meta-test respectively, few methods [10, 24, 25] perform both feature selection in meta-training and also finetuning their feature selection mechanisms in meta-testing.

Recently Li *et al.* [22] has tackled the first challenge by distilling information from multiple domain-specific networks into a single network without requiring any feature selection step. The authors show that the learned representations are *universal* and can be directly transferred to few-shot tasks in previously unseen domains and outperform the prior feature selection based methods [10, 24] while being more computationally efficient in test time. In this paper, we build on their success and solely focus on addressing the second challenge and propose to leverage the information in few support samples for model adaptation.

To this end, we study efficient adaptation strategies in meta-test phase that can be easily incorporated to state-of-the-art methods with minimum computational increase. In particular, we rigorously investigate the use of different adapter types [33, 34], conditioning mechanisms [35] along with matrix decomposition and evaluate the design choices in terms of performance and computation tradeoff. We show that the best proposed strategy, *residual adaptation in meta-test*, which has not been previously explored by any prior work, achieves the state-of-the-art performance in most domains, especially resulting in superior performance in unseen domains on Meta-Dataset with negligible increase in computations.

2 Related Work

Few-shot learning is an extensively studied problem in computer vision. For the methods that focus on homogeneous few-shot tasks, we refer to [14, 46] for comprehensive review. We focus on the more challenging setting of multi-domain few-shot tasks on Meta-Dataset [23]. The previous work in this problem can be broadly grouped into two groups, learning to transfer related domain knowledge in meta-training and model adaptation in meta-testing.

Domain knowledge transfer in meta-training. CNAPS [35] learns a task encoder to modulate feature extractor with FiLM layers [36] and also adapts the classifier with new samples. Simple CNAPS [35] improves CNAPS by replacing its classifier with a non-parametric classifier based on Mahalanobis distance. Transductive CNAP [2] extends the few-shot setting to a transductive setting where the query set is exploited to boost its performance. Both SUR [10] and URT [24] first train an independent network for each domain and then a fusion strategy is further proposed to fuse features from all domains to adapt to unseen domains. FLUTE [25] learns a shared backbone network for all domains with a specific modulator for each domain during meta-training. Domain modulators are later fused with an auxiliary “blending network” to initialize for new tasks in meta-test. URL [2] learns a single multi-domain network by distilling the knowledge of domain-specific networks. In fact, we build our method on URL due to its high performance and simplicity.

Model adaptation for meta-test. Non-parametric classifiers such as nearest centroid classifier (NCC) and its variants [33, 34] are commonly used in few-shot tasks due to their simplicity and do not require further adaptation at meta-test. Meta-Baseline [8] and Baseline [9] fine-tune the whole model during meta-test, while Baseline++ [8] only updates a parametric classifier with the cosine distance, RFS [21] learns a linear classifier with Logistic regression and MetaOptNet [21] optimizes a linear support vector machine (SVM). MAML [22] and

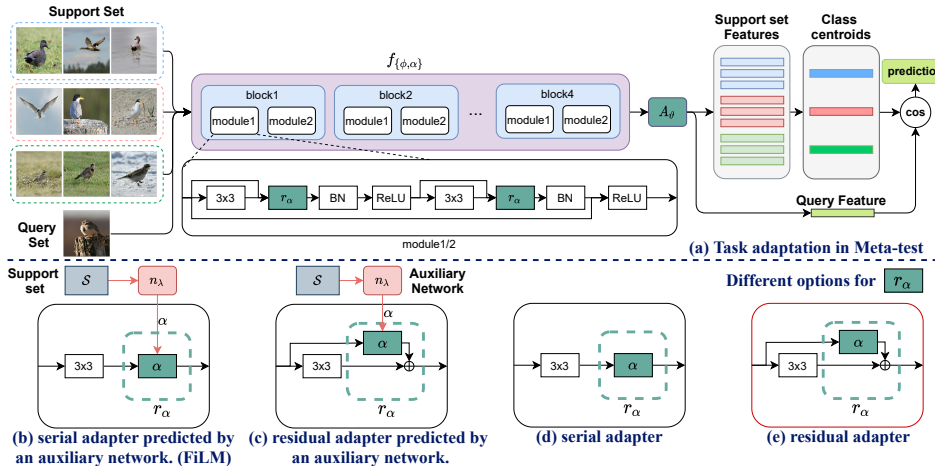


Figure 1: Illustration of our task adaptation for cross-domain few-shot learning. In meta-test stage (a), our method first attaches a parametric transformation r_α to each layer, where α can be modeled as (b) prediction of an auxiliary network or (e) learnable parameters. r_α can be constructed by (d) a serial or (e) a residual adaptation. We found that (e) is the best configuration which is further improved by attaching a linear transformation A_θ to the end of the network. We adapt the network for a given task by optimizing α and A_θ on a few labeled images from the support set, then map query images to the task-specific space and assign them to the nearest class center.

LEO [35] meta-learn how to update parameters during meta-test. TADAM [24] employs a task embedding network to predict scaling and shifting parameters for each convolutional layer, similarly more dedicated methods are proposed for multi-domain few-shot generalization with a task encoder to generate conditioning parameters [11, 12, 25, 26].

There are also methods (e.g. [11, 33]) that do not fit into this grouping. BOHB [33] proposes to use multi-domain data as validation objective for hyper-parameter optimization. CTX [10] proposes to learn spatial correspondences from ImageNet and evaluates on the remaining domains as unseen domains. As they both only learn representations from a single domain (ImageNet), their results are not directly comparable to ours.

3 Method

Few-shot learning aims at learning to classify samples of new categories efficiently from a small training set with only few samples for each class. Each few-shot learning task consists of a support set $\mathcal{S} = \{(\mathbf{x}_i, y_i)\}_{i=1}^{|\mathcal{S}|}$ with $|\mathcal{S}|$ sample and label pairs respectively and a query set $\mathcal{Q} = \{(\mathbf{x}_j)\}_{j=1}^{|\mathcal{Q}|}$ with $|\mathcal{Q}|$ samples to be classified. The goal is to learn a classifier on \mathcal{S} that accurately predicts the labels of \mathcal{Q} .

As in [10, 22, 24], we solve this problem in two steps: i) representation learning where we learn a general feature extractor f from a large dataset \mathcal{D}_b , ii) adaptation where the target tasks $(\mathcal{S}, \mathcal{Q})$ are sampled from another large dataset \mathcal{D}_t by taking the subsets of the dataset to build \mathcal{S} and \mathcal{Q} . Note that \mathcal{D}_b and \mathcal{D}_t contain mutually exclusive classes.

3.1 Representation learning from multiple domains

Learning domain-agnostic or universal representations [3] has been key to the success of cross-domain generalization. While representations learned from a large diverse dataset such as ImageNet can be considered as universal and successfully transferred to tasks in different domains with minor adaptations [10, 24, 30], recent work [22] shows that learning a single set of representations over multiple domains is more effective in cross-domain few-shot learning. Hence we adopt the multi-domain network in [22] that consists of a single feature extractor shared across all domains and use it as a feature extractor for the unseen few-shot tasks.

Let assume that $\mathcal{D}_b = \{\mathcal{D}_\tau\}_{\tau=1}^T$ consists of T subdatasets, each sampled from a different domain. The vanilla multi-domain learning (MDL) strategy jointly optimizes network parameters over the images from all T domains (datasets):

$$\min_{\phi, \psi_\tau} \sum_{\tau=1}^T \frac{1}{|\mathcal{D}_\tau|} \sum_{\mathbf{x}, y \in \mathcal{D}_\tau} \ell(g_{\psi_\tau} \circ f_\phi(\mathbf{x}), y), \quad (1)$$

where ℓ is cross-entropy loss, f is a multi-domain feature extractor that takes an image as input and outputs a d dimensional feature and is parameterized by a single set of parameters ϕ which is shared across T domains. g_{ψ_τ} is the classifier for domain τ parameterized by ψ and is discarded during meta-test. The challenge here is to share the knowledge across the domains while preventing negative transfer between them and also carefully balancing the individual loss functions ([10]). URL [22] mitigates these challenges by first training an individual domain-specific network offline and then distilling their knowledge into a single multi-domain network. We refer readers to [22] for more details.

3.2 Task adaptation for few-shot learning

Though the multi-domain model f_ϕ can produce representations that generalize to many previously unseen domains, this gets more challenging when there is a large domain gap between the training set \mathcal{D}_b and test tasks drawn from \mathcal{D}_t . To this end, we focus on adapting the model to unseen classes and domains by attaching task-specific parameters to the model.

Simple task adaptation techniques are finetuning all the model parameters ϕ [6, 9], learning only parameters of a linear classifier [21] or of a high-dimensional mapping [22] on few support samples. However, these strategies have shortcomings due to either the contrast between the small number of support samples and large number of parameters to be updated or the limited capacity of learned (linear) transformations. To address these limitations, here we propose more effective adaptation strategies, inspired from [1, 2, 31, 32, 33, 35, 36], that can modulate task-specific information while transferring the previously learned knowledge from multiple domains, and efficiently learn to transform the visual representations from few samples. More specifically, let f_w denote a layer of the multi-domain network f_ϕ (*i.e.* a convolutional layer) with the weights w . Given a support set \mathcal{S} , the task-specific adaptation can be incorporated to the output of the layer f_w as

$$f_{\{w, \alpha\}}(\mathbf{h}) = r_\alpha(f_w(\mathbf{h}), \mathbf{h}) \quad (2)$$

where $\mathbf{h} \in \mathbb{R}^{W \times H \times C}$ is the input tensor, f_w is a convolutional layer in f_ϕ and r_α is a simple parametric transformation. Importantly, the number of the task specific adaptation parameters α are significantly smaller than the multi-domain network ones. Estimation of α and design of the transformation r_α can be realized in different ways.

Predicting α . After freezing the network parameters ϕ , we focus on two options for estimating α . In the first case, as adopted by several methods [11, 12, 13, 14], we use an auxiliary network or a task encoder n_λ with parameters λ to predict α values for a given support set (illustrated in Fig. 1(b) and (c)). In particular, n takes in the support set as input and outputs an α for each layer of network f . In words, the auxiliary network adapts f_w dynamically to variations of the support set. Here λ are learned in meta-train from the training set \mathcal{D}_b and fixed during meta-test. In the second case (illustrated in Fig. 1(d) and (e)), which we found achieving superior performance, the task specific parameters α can be directly attached to f_w and learned from scratch on the support set in meta-test without using the task encoder, thanks to their small capacity.

Designing r_α architecture. Next we propose two options for how to connect r_α to f_w : i) serial connection by subsequently applying it to the output of layer $f_w(\mathbf{h})$ as $f_{\{w,\alpha\}}(\mathbf{h}) = r_\alpha \circ f_w(\mathbf{h})$ (illustrated in Fig. 1(b) and (d)), ii) parallel connection by a residual addition $f_{\{w,\alpha\}}(\mathbf{h}) = f_w(\mathbf{h}) + r_\alpha(\mathbf{h})$ (illustrated in Fig. 1(c) and (e)) as in [33]. We found the parallel setting performing the best with learnable parameters α when learned from scratch during meta-test which we discuss in Section 4 and is illustrated in Fig. 1(e).

Designing r_α parameterization. For the parameterization of r_α , we consider two options: i) matrix multiplication with $\alpha \in \mathbb{R}^{C \times C}$, ii) channelwise scaling ($\alpha \in \mathbb{R}^C$). While the matrix multiplication is more powerful than the scaling operation, it also requires more parameters to be estimated or learned (*i.e.* C^2 vs C). Note that, in a deep neural network, the number of input C_{in} and output channels C_{out} for a layer can be different. In that case, one can still use a non-square matrix: $\alpha \in \mathbb{R}^{C_{\text{out}} \times C_{\text{in}}}$, however, it is not possible to use a scaling operator in the parallel setting. In our experiments, we use ResNet architecture [13] where most input and output channels are the same. Note that r_α with learnable parameters α connected in parallel with matrix multiplication form is known as residual adapter [33] and r_α implemented as a prediction of an auxiliary network connected serial in channelwise is known as FiLM [34].

An alternative way to reduce the dimensionality of α in case of matrix multiplication is matrix decomposition: $\alpha = \beta \gamma^\top$, where $\beta \in \mathbb{R}^{C \times K}$ and $\gamma \in \mathbb{R}^{C \times K}$, $K \ll C$. Using a bottleneck, *i.e.* setting $K < C/2$, reduces the number of parameters in the multiplication. In this work, we set $K = [C/N]$ and evaluate the performance for various N in Section 4. Note that the matrix multiplication is implemented as a convolutional operation with 1×1 kernels in our code.

Pre-classifier alignment. Finally, we use an additional adaptation layer that takes in the features that are computed from the network with the task-specific adaptation $f_{\{\phi,\alpha\}} \in \mathbb{R}^d$ and apply an affine transformation $A_\vartheta : \mathbb{R}^d \rightarrow \mathbb{R}^d$ parameterized by $\vartheta \in \mathbb{R}^{d \times d}$ to obtain the network embedding $\mathbf{z} = A_\vartheta \circ f_{\{\phi,\alpha\}}$. This additional transformation is learned from the support set, shown to map the features to a more discriminative space and thus boosts its classification performance as shown in [27].

3.3 Learning to adapt

We build our model on the commonly used nearest centroid classifier (NCC) [76] as in [11, 12, 13] by averaging the embeddings belonging to each class: $\mathbf{c}_j = \frac{1}{|\mathcal{S}_j|} \sum_{\mathbf{z}_i \in \mathcal{S}_j} \mathbf{z}_i$ where $\mathcal{S}_j = \{\mathbf{z}_k : y_k = j\}$, $j = 1, \dots, N_c$ and N_c is the number of classes in the support set. Next we estimate the likelihood of a support sample \mathbf{z} by:

$$p(y = l | \mathbf{z}) = \frac{\exp(-d(\mathbf{z}, \mathbf{c}_l))}{\sum_{j=1}^{N_c} \exp(-d(\mathbf{z}, \mathbf{c}_j))}, \quad (3)$$

where $d(\mathbf{z}, \mathbf{c}_l)$ is the negative cosine similarity.

To optimize the attached adaptation parameters α during meta-test, we minimize the following objective w.r.t. α and ϑ :

$$\min_{\alpha, \vartheta} \frac{1}{|\mathcal{S}|} \sum_{\mathbf{x}_i, y_i \in \mathcal{S}} [\log(p(y = y_i | \mathbf{x}_i))]. \quad (4)$$

where \mathcal{S} is sampled from the test set \mathcal{D}_t . We then use $f_{\{\phi, \alpha\}}$ to extract features of query samples and use ϑ and Eq. (3) to predict the label of each query sample from \mathcal{Q} by assigning the label of the closest centroid \mathbf{c}_j . Our meta-test pipeline is illustrated in Fig. 1(a).

4 Experiments

Here we first describe the benchmarks, implementation details and competing methods. Then we rigorously compare our method to the state-of-the-art, study each proposed component in an ablation, also provide a qualitative analysis of our results.

4.1 Experimental setup

Dataset. We use the Meta-Dataset [43] that contains data from 13 datasets in all our experiments, follow the standard evaluation procedure and include more details in the supplementary.

Implementation details. We use PyTorch [30] to implement our method and will make the code available. As in [2, 10, 22], we build our method on ResNet-18 [13] backbone in all experiments. We follow [22] to train a multi-domain network on the training set by using a SGD optimizer with a momentum and the cosine annealing learning scheduler with the same hyperparameters. Once learned, we freeze its parameters and experiment with various adaptation strategies. In the case of learnable adapter parameters α (see Fig. 1(d) and (e)), we learn them from scratch along with ϑ for 40 iterations using Adadelta [27] on the support samples in meta-test. In the case of the auxiliary network (see Fig. 1(b) and (c))), we learn its parameters λ in meta-train.

4.2 Results

Comparisons of different r_α choices. Here we evaluate the design choices for r_α that are explained in Section 3. The first group includes baselines without any adaptation parameters but only non-parametric classifiers including nearest centroid classifier (NCC) and NCC Mahalanobis Distance (MD), without r_α but parametric classifiers including logistic regression (LR), support vector machine SVM whose parameters are learning from support samples, and finetuning with NCC. The second group involves adaptation through an auxiliary network (*Aux-Net*) as task encoder with different classifiers (NCC, MD), connection types (serial, residual) and channelwise modulation (CW). Note that in this setting, we do not include the pre-classifier adaptation, as it involves learning only in meta-training. The next group involves adaptation through adapters (*Ad*) with serial and residual connections, in channelwise and matrix (*M*) forms, and with and without preclassifier alignment (PA). We built all these variants on the multi-domain URL feature extractor [22] learned during meta-training and report the results in Table 1.

First we observe that NCC obtains the best results for the seen domains and its performance is further improved by MD, while SVM achieves the best for the unseen domains in the first group. Finetuning baseline provides competitive results especially for the unseen domains. However, it performs poor in most seen domains. In case of modulating α with the

auxiliary network, MD outperforms NCC for the unseen domains as expected. The parallel configuration (FiLM-R) works significantly better than the serial counterpart (FiLM-S). Note that FiLM-S with MD corresponds to Simple CNAPS [53] with the more competitive URL features.

Next we observe that using learnable α parameters through adapters in both serial (Ad-S) and residual ways (Ad-R) outperforms the auxiliary baseline in most seen domains and especially in the unseen ones with a large margin. This strongly suggests that learning adapter parameters directly from support samples is more effective than estimating them via an auxiliary network. In addition, the auxiliary network contains significantly more additional parameters than the ones of adapters for a given task (77% vs 0.06-12.5%). In this setting, residual adapters (Ad-R) performs the best when combined with the adapters in matrix form (Ad-R-M). Finally using the pre-classifier alignment (Ad-R-CW-PA and Ad-R-M-PA) further boosts the performance of the best models. While these two models together achieve the best performance in 10 out of 12 domains, the channelwise model (Ad-R-CW-PA) provides a remarkable performance with only 4% increase in number of parameters.

Test Dataset	classifier	Aux-Net or Ad	serial or residual	M or CW	ϑ	#params	Image-Net	Omni-glot	Air-craft	Birds	Textures	Quick Draw	Fungi	VGG Flower	Traffic Sign	MS-COCO	MNIST	CIFAR-10	CIFAR-100
NCC	NCC	-	-	-	\times	-	57.0	94.4	88.0	80.3	74.6	81.8	66.2	91.5	49.8	54.1	91.1	70.6	59.1
MD	MD	-	-	-	\times	-	53.9	93.8	87.6	78.3	73.7	80.9	57.7	89.7	62.2	48.5	95.1	68.9	60.0
LR	LR	-	-	-	\times	-	56.0	93.7	88.3	79.7	74.7	80.0	62.1	91.1	59.7	51.2	93.5	73.1	60.1
SVM	SVM	-	-	-	\times	-	54.5	94.3	87.7	78.1	73.8	80.0	58.5	91.4	65.7	50.5	95.4	72.0	60.5
Finetune	NCC	-	-	-	\times	-	55.92	94.05	87.36	77.89	76.88	75.39	57.61	91.56	86.19	53.12	96.84	80.98	65.91
FiLM-S	NCC	Aux-Net	serial	CW	\times	76.98%	54.6	93.5	86.6	78.6	71.5	79.3	66.0	87.6	43.3	49.1	87.9	62.8	51.5
FiLM-R	NCC	Aux-Net	residual	CW	\times	76.98%	56.1	94.2	88.4	80.6	74.9	82.0	66.4	91.6	48.5	53.5	90.8	70.2	59.7
FiLM-S	MD	Aux-Net	serial	CW	\times	76.98%	55.1	93.8	86.8	77.4	73.2	79.9	57.4	88.1	58.4	50.1	92.7	66.5	55.7
FiLM-R	MD	Aux-Net	residual	CW	\times	76.98%	54.8	93.8	87.4	78.2	73.4	81.1	58.8	90.1	63.6	48.5	94.8	69.6	60.6
Ad-S-CW	NCC	Ad	serial	CW	\times	0.06%	56.8	94.8	89.3	80.7	74.5	81.6	65.8	91.3	73.9	53.6	95.7	78.4	64.3
Ad-R-CW (Ours)	NCC	Ad	residual	CW	\times	1.57%	57.6	94.7	89.0	81.2	75.2	81.5	65.4	91.8	79.2	54.7	96.4	79.5	67.4
Ad-S-M	NCC	Ad	serial	M	\times	12.50%	56.2	94.4	89.1	80.6	75.8	81.6	67.1	92.1	67.6	54.8	95.9	78.9	66.6
Ad-R-M (Ours)	NCC	Ad	residual	M	\times	10.93%	57.3	94.9	88.9	81.0	76.7	80.6	65.4	91.4	82.6	55.0	96.6	82.1	66.4
Ad-R-CW-PA (Ours)	NCC	Ad	residual	CW	\checkmark	3.91%	58.6	94.5	90.0	80.5	77.6	81.9	67.0	92.2	80.2	57.2	96.1	81.5	71.4
Ad-R-M-PA (Ours)	NCC	Ad	residual	M	\checkmark	13.27%	59.5	94.9	89.9	81.1	77.5	81.7	66.3	92.2	82.8	57.6	96.7	82.9	70.4

Table 1: Comparisons to methods that learn classifiers and model adaptation methods during meta-test stage based on URL model. NCC, MD, LR, SVM denote nearest centroid classifier, Mahalanobis distance, logistic regression, support vector machines respectively. ‘Aux-Net or Ad’ indicates using Auxiliary Network to predict α or attaching adapter α directly. ‘M or CW’ means using matrix multiplication or channel-wise scaling adapters. ‘S’ and ‘R’ denote serial adapter and residual adapter, respectively. ‘ ϑ ’ indicates using the pre-classifier adaptation. The standard deviation results can be found in the supplementary. The first eight datasets are seen during training and the last five datasets are unseen and used for test only.

Our method with different feature extractors. Table 2 shows the results of our method (Ad-R-M-PA) when incorporated to different feature extractors, single domain model (SDL) pre-trained on ImageNet, vanilla multi-domain learning (MDL, see Eq. (1)) and URL [22]. We see that attaching and learning residual adapters can significantly improve the performance on all domains over SDL and MDL and obtain better performance on most domains over URL (11 out of 13 domains). This strongly indicates that our method can efficiently adapt the model for unseen categories and domains with few support samples while being agnostic to the feature extractor.

Comparisons with recent state-of-the-art methods. We then compare our method (Ad-R-M-PA) with the URL features to the state-of-the-art methods in Table 3 (CNAPS [53], SUR [10], URT [24], Simple CNAPS [9], Transductive CNAPS [10], FLUTE [42], and URL [22]). To better analyze the results, we also report the average accuracy on seen domains, unseen domains, all domains and the average rank as in [22, 42]. From the results,

Test Dataset	ImageNet	Omniglot	Aircraft	Birds	Textures	Quick Draw	Fungi	VGG Flower	Traffic Sign	MSCOCO	MNIST	CIFAR-10	CIFAR-100
SDL	55.8 \pm 1.0	67.4 \pm 1.2	49.5 \pm 0.9	71.2 \pm 0.9	73.0 \pm 0.6	53.9 \pm 1.0	41.6 \pm 1.0	87.0 \pm 0.6	47.4 \pm 1.1	53.5 \pm 1.0	78.1 \pm 0.7	67.3 \pm 0.8	56.6 \pm 0.9
Ours (SDL)	59.5 \pm 1.1	78.2 \pm 1.2	72.2 \pm 1.0	74.9 \pm 0.9	77.3 \pm 0.7	67.6 \pm 0.9	44.7 \pm 1.0	90.9 \pm 0.6	82.5 \pm 0.8	59.0 \pm 1.0	93.9 \pm 0.6	82.1 \pm 0.7	70.7 \pm 0.9
MDL	53.4 \pm 1.1	93.8 \pm 0.4	86.6 \pm 0.5	78.6 \pm 0.8	71.4 \pm 0.7	81.5 \pm 0.6	61.9 \pm 1.0	88.7 \pm 0.6	51.0 \pm 1.0	49.7 \pm 1.1	94.4 \pm 0.3	66.7 \pm 0.8	53.6 \pm 1.0
Ours (MDL)	55.6 \pm 1.0	94.3 \pm 0.4	86.7 \pm 0.5	79.4 \pm 0.8	73.2 \pm 0.8	81.7 \pm 0.6	64.0 \pm 0.9	90.9 \pm 0.5	81.1 \pm 0.9	51.4 \pm 1.1	96.9 \pm 0.3	78.5 \pm 0.8	64.3 \pm 1.1
URL [21]	58.8 \pm 1.1	94.5 \pm 0.4	89.4 \pm 0.4	80.7 \pm 0.8	77.2 \pm 0.7	82.5 \pm 0.6	68.1 \pm 0.9	92.0 \pm 0.5	63.3 \pm 1.2	57.3 \pm 1.0	94.7 \pm 0.4	74.2 \pm 0.8	63.6 \pm 1.0
Ours (URL)	59.5 \pm 1.0	94.9 \pm 0.4	89.9 \pm 0.4	81.1 \pm 0.8	77.5 \pm 0.7	81.7 \pm 0.6	66.3 \pm 0.9	92.2 \pm 0.5	82.8 \pm 1.0	57.6 \pm 1.0	96.7 \pm 0.4	82.9 \pm 0.7	70.4 \pm 1.0

Table 2: Results of attaching residual adapters to different baselines. ‘SDL’ is the single domain model pretrained on ImageNet. ‘MDL’ is a vanilla Multi-Domain Learning (MDL) model trained on eight seen datasets jointly.

our method outperforms other methods on most domains (10 out of 13), especially obtaining significant improvement on 5 unseen datasets than the second best method, *i.e.* Average Unseen (+7.5). More specifically, our method obtains significant better results than the second best approach on Traffic Sign (+19.5), CIFAR-10 (+8.7), and CIFAR-100 (+6.8). Achieving improvements on previously unseen datasets is more challenging due to a large generalization gap between seen training datasets and unseen testing datasets and this results again verify the efficacy of our method on adapting features for unseen few-shot learning tasks.

Test Dataset	CNAPS [20]	Best SDL	MDL	Simple CNAPS [20]	TransductiveCNAPS [20]	SUR [20]	URT [20]	FLUTE [20]	URL [20]	Ours
ImageNet	50.8 \pm 1.1	55.8 \pm 1.0	53.4 \pm 1.1	58.4 \pm 1.1	57.9 \pm 1.1	56.2 \pm 1.00	56.8 \pm 1.1	51.8 \pm 1.1	58.8 \pm 1.1	59.5 \pm 1.0
Omniglot	91.7 \pm 0.5	93.2 \pm 0.5	93.8 \pm 0.4	91.6 \pm 0.6	94.3 \pm 0.4	94.1 \pm 0.42	94.2 \pm 0.4	93.2 \pm 0.5	94.5 \pm 0.4	94.9 \pm 0.4
Aircraft	83.7 \pm 0.6	85.7 \pm 0.5	86.6 \pm 0.5	82.0 \pm 0.7	84.7 \pm 0.5	85.5 \pm 0.54	85.8 \pm 0.5	87.2 \pm 0.5	89.4 \pm 0.4	89.9 \pm 0.4
Birds	73.6 \pm 0.9	71.2 \pm 0.9	78.6 \pm 0.8	74.8 \pm 0.9	78.8 \pm 0.7	71.0 \pm 1.00	76.2 \pm 0.8	79.2 \pm 0.8	80.7 \pm 0.8	81.1 \pm 0.8
Textures	55.9 \pm 0.7	73.0 \pm 0.6	71.4 \pm 0.7	68.8 \pm 0.6	66.2 \pm 0.8	71.0 \pm 0.80	71.6 \pm 0.7	68.8 \pm 0.8	77.2 \pm 0.7	77.5 \pm 0.7
Quick Draw	74.7 \pm 0.8	82.8 \pm 0.6	81.5 \pm 0.6	76.5 \pm 0.8	77.9 \pm 0.6	81.8 \pm 0.57	82.4 \pm 0.6	79.5 \pm 0.7	82.5 \pm 0.6	81.7 \pm 0.6
Fungi	50.2 \pm 1.1	65.8 \pm 0.9	61.9 \pm 1.0	46.6 \pm 1.0	48.9 \pm 1.2	64.3 \pm 0.95	64.0 \pm 1.0	58.1 \pm 1.1	68.1 \pm 0.9	66.3 \pm 0.9
VGG Flower	88.9 \pm 0.5	87.0 \pm 0.6	88.7 \pm 0.6	90.5 \pm 0.5	92.3 \pm 0.4	82.9 \pm 0.78	87.9 \pm 0.6	91.6 \pm 0.6	92.0 \pm 0.5	92.2 \pm 0.5
Traffic Sign	56.5 \pm 1.1	47.4 \pm 1.1	51.0 \pm 1.0	57.2 \pm 1.0	59.7 \pm 1.1	51.0 \pm 1.11	48.3 \pm 1.1	58.4 \pm 1.1	63.3 \pm 1.2	82.8 \pm 1.0
MSCOCO	39.4 \pm 1.0	53.5 \pm 1.0	49.7 \pm 1.1	48.9 \pm 1.1	42.5 \pm 1.1	52.0 \pm 1.09	51.5 \pm 1.1	50.0 \pm 1.0	57.3 \pm 1.0	57.6 \pm 1.0
MNIST	-	89.8 \pm 0.5	94.4 \pm 0.3	94.6 \pm 0.4	95.7 \pm 0.3	94.3 \pm 0.41	90.6 \pm 0.5	95.6 \pm 0.5	94.7 \pm 0.4	96.7 \pm 0.4
CIFAR-10	-	67.3 \pm 0.8	66.7 \pm 0.8	74.9 \pm 0.7	75.7 \pm 0.7	66.5 \pm 0.89	67.0 \pm 0.8	78.6 \pm 0.7	74.2 \pm 0.8	82.9 \pm 0.7
CIFAR-100	-	56.6 \pm 0.9	53.6 \pm 1.0	61.3 \pm 1.1	62.9 \pm 1.0	56.9 \pm 1.10	57.3 \pm 1.0	67.1 \pm 1.0	63.6 \pm 1.0	70.4 \pm 1.0
Average Seen	71.6	76.8	77.0	73.7	75.1	75.9	77.4	76.2	80.4	80.4
Average Unseen	-	62.9	63.1	67.4	67.3	64.1	62.9	69.9	70.6	78.1
Average All	-	71.5	71.6	71.2	72.1	71.4	71.8	73.8	76.6	79.5
Average Rank	-	6.1	6.0	6.4	5.4	6.1	5.8	5.0	2.4	1.8

Table 3: Comparison to baselines and state-of-the-art methods on Meta-Dataset. Mean accuracy, 95% confidence interval are reported. The first eight datasets are seen during training and the last five datasets are unseen and used for test only.

4.3 Further results

Varying-way Five-shot. After evaluating our method over a broad range of varying shots (*e.g.* up to 100 shots), we follow [20, 21] to further analyze our method in 5-shot setting of varying number of categories. In this setting, we sample a varying number of ways with a fixed number of shots to form balanced support and query sets. As shown in Table 4, overall performance for all methods decreases in most datasets compared to results in Table 3 indicating that this is a more challenging setting. It is due to that five-shot setting samples much less support images per class than the standard setting. The top-2 methods remain the same and ours still outperforms the state-of-the-art URL when the number of support images per class is fewer, especially on unseen domains (Average Unseen +6.2).

Five-way One-shot. The similar conclusion can be drawn from this challenging setting. Note that there are extremely few samples available for training in this case. As we can see, Ours achieves similar results with URL on seen domains but much better performance on unseen domains. The reason is that learning the attached residual adapters is less over-fitting.

Test Dataset	Varying-Way Five-Shot					Five-Way One-Shot				
	Simple CNAPS	SUR	URT	URL	Ours	Simple CNAPS	SUR	URT	URL	Ours
Average Seen	69.0	71.2	73.8	76.6	76.7	65.0	64.0	70.6	73.4	73.5
Average Unseen	62.6	56.0	59.6	65.2	71.4	57.7	49.6	57.5	62.4	63.4
Average All	66.5	65.4	68.3	72.2	74.6	62.2	58.5	65.5	69.2	69.6
Average Rank	4.1	3.9	3.4	2.1	1.5	3.8	4.5	3.3	1.7	1.7

Table 4: Results of Varying-Way Five-Shot and Five-Way One-Shot scenarios. Mean accuracies are reported and more detailed results can be found in the supplementary.

4.4 Ablation study

Here, we conduct ablation study for the sensitivity analysis for number of iterations, layer analysis for adapters, and decomposed residual adapters. We summarize results in figures and we refer to supplementary for more detailed results.

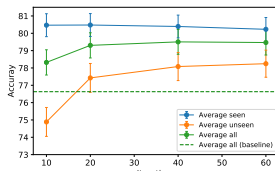


Figure 2: Sensitivity of per-
iteration performance to number of iterations.

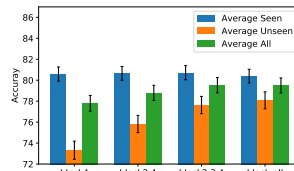


Figure 3: Block (layer) analysis for adapters.

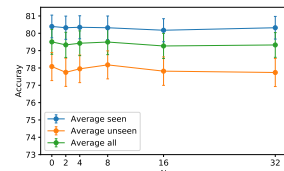


Figure 4: Decomposed residual adapters on block-3,4.

Sensitivity analysis for number of iterations. In our method, we optimize the attached parameters (α, ϑ) with 40 iterations. Figure 2 reports the results with 10, 20, 40, 60 iterations and indicates that our method (solid green) converges to a stable solution after 20 iterations and achieves better average performance on all domains than the baseline URL (dash green).

Layer analysis for adapters. Here we investigate whether it is sufficient to attach the adapters only to the later layers. We evaluate this on ResNet18 which is composed of four blocks and attach the adapters to only later blocks (block4, block3,4, block2,3,4 and block-all, see Fig. 1). Figure 3 shows that applying our adapters to only the last block (block4) obtains around 78% average accuracy on all domains which outperforms the URL. With attaching residual adapters to more layers, the performance on unseen domains is improved significantly while the one on seen domains remains stable.

Decomposing residual adapters. Here we investigate whether one can reduce the number of parameters in the adapters while retaining its performance by using matrix decomposition (see Section 3). As in deep neural network, the adapters in earlier layers are relatively small, we then decompose the adapters in the last two blocks only where the adapter dimensionality goes up to 512×512 . Figure 4 shows that our method can achieve good performance with less parameters by decomposing large residual adapters, (e.g. when $N = 32$ where the number of additional parameters equal to around 4% vs 13%, the performance is still comparable to the original form of residual adapters, *i.e.* $N=0$). We refer to supplementary for more detailed results and explanation.

5 Conclusion

In this work, we investigate various strategies for adapting deep networks to few-shot classification tasks and show that light-weight adapters connected to a deep network with residual connections achieves strong adaptation to new tasks and domains only from few samples and obtains state-of-the-art performance while being efficient in the challenging Meta-Dataset benchmark. The proposed solution can be incorporated to various feature extractors and leads to a negligible increase in number of parameters.

References

- [1] P. Bateni, J. Barber, J.-W. van de Meent, and F. Wood. Enhancing few-shot image classification with unlabelled examples. *arXiv preprint arXiv:2006.12245*, 2020.
- [2] P. Bateni, R. Goyal, V. Masrani, F. Wood, and L. Sigal. Improved few-shot visual classification. In *CVPR*, pages 14493–14502, 2020.
- [3] H. Bilen and A. Vedaldi. Universal representations: The missing link between faces, text, planktons, and cat breeds. *arXiv preprint arXiv:1701.07275*, 2017.
- [4] S. Brigit and C. Yin. Fgvcx fungi classification challenge. *online*, 2018.
- [5] W.-Y. Chen, Y.-C. Liu, Z. Kira, Y.-C. F. Wang, and J.-B. Huang. A closer look at few-shot classification. In *ICLR*, 2019.
- [6] Y. Chen, X. Wang, Z. Liu, H. Xu, and T. Darrell. A new meta-baseline for few-shot learning. *arXiv preprint arXiv:2003.04390*, 2020.
- [7] Z. Chen, V. Badrinarayanan, C.-Y. Lee, and A. Rabinovich. Gradnorm: Gradient normalization for adaptive loss balancing in deep multitask networks. In *ICML*, pages 794–803. PMLR, 2018.
- [8] M. Cimpoi, S. Maji, I. Kokkinos, S. Mohamed, and A. Vedaldi. Describing textures in the wild. In *CVPR*, pages 3606–3613, 2014.
- [9] G. S. Dhillon, P. Chaudhari, A. Ravichandran, and S. Soatto. A baseline for few-shot image classification. In *ICLR*, 2020.
- [10] C. Doersch, A. Gupta, and A. Zisserman. Crosstransformers: spatially-aware few-shot transfer. In *NeurIPS*, 2020.
- [11] N. Dvornik, C. Schmid, and J. Mairal. Selecting relevant features from a multi-domain representation for few-shot classification. In *ECCV*, pages 769–786, 2020.
- [12] C. Finn, P. Abbeel, and S. Levine. Model-agnostic meta-learning for fast adaptation of deep networks. In *ICLR*, pages 1126–1135, 2017.
- [13] K. He, X. Zhang, S. Ren, and J. Sun. Deep residual learning for image recognition. In *CVPR*, pages 770–778, 2016.
- [14] T. Hospedales, A. Antoniou, P. Micaelli, and A. Storkey. Meta-learning in neural networks: A survey. *arXiv preprint arXiv:2004.05439*, 2020.
- [15] S. Houben, J. Stallkamp, J. Salmen, M. Schlipsing, and C. Igel. Detection of traffic signs in real-world images: The german traffic sign detection benchmark. In *IJCNN*, pages 1–8. Ieee, 2013.
- [16] J. Jongejan, R. Henry, K. Takashi, K. Jongmin, and F.-G. Nick. The quick, draw! a.i. experiment. *online*, 2016.
- [17] A. Krizhevsky, G. Hinton, et al. Learning multiple layers of features from tiny images. *Citeseer*, 2009.
- [18] B. Lake, R. Salakhutdinov, J. Gross, and J. Tenenbaum. One shot learning of simple

- visual concepts. In *Proceedings of the annual meeting of the cognitive science society*, volume 33, 2011.
- [19] B. M. Lake, R. Salakhutdinov, and J. B. Tenenbaum. Human-level concept learning through probabilistic program induction. *Science*, 350(6266):1332–1338, 2015.
- [20] Y. LeCun, L. Bottou, Y. Bengio, and P. Haffner. Gradient-based learning applied to document recognition. *Proceedings of the IEEE*, 86(11):2278–2324, 1998.
- [21] K. Lee, S. Maji, A. Ravichandran, and S. Soatto. Meta-learning with differentiable convex optimization. In *CVPR*, pages 10657–10665, 2019.
- [22] W.-H. Li, X. Liu, and H. Bilen. Universal representation learning from multiple domains for few-shot classification. *arXiv preprint arXiv:2103.13841*, 2021.
- [23] T.-Y. Lin, M. Maire, S. Belongie, J. Hays, P. Perona, D. Ramanan, P. Dollár, and C. L. Zitnick. Microsoft coco: Common objects in context. In *ECCV*, pages 740–755. Springer, 2014.
- [24] L. Liu, W. Hamilton, G. Long, J. Jiang, and H. Larochelle. A universal representation transformer layer for few-shot image classification. In *ICLR*, 2021.
- [25] S. Maji, E. Rahtu, J. Kannala, M. Blaschko, and A. Vedaldi. Fine-grained visual classification of aircraft. *arXiv preprint arXiv:1306.5151*, 2013.
- [26] T. Mensink, J. Verbeek, F. Perronnin, and G. Csurka. Distance-based image classification: Generalizing to new classes at near-zero cost. *TPAMI*, 35(11):2624–2637, 2013.
- [27] E. G. Miller, N. E. Matsakis, and P. A. Viola. Learning from one example through shared densities on transforms. In *CVPR*, volume 1, pages 464–471. IEEE, 2000.
- [28] M.-E. Nilsback and A. Zisserman. Automated flower classification over a large number of classes. In *2008 Sixth Indian Conference on Computer Vision, Graphics & Image Processing*, pages 722–729. IEEE, 2008.
- [29] B. N. Oreshkin, P. Rodriguez, and A. Lacoste. Tadam: Task dependent adaptive metric for improved few-shot learning. In *NeurIPS*, 2018.
- [30] A. Paszke, S. Gross, F. Massa, A. Lerer, J. Bradbury, G. Chanan, T. Killeen, Z. Lin, N. Gimelshein, L. Antiga, A. Desmaison, A. Kopf, E. Yang, Z. DeVito, M. Raison, A. Tejani, S. Chilamkurthy, B. Steiner, L. Fang, J. Bai, and S. Chintala. Pytorch: An imperative style, high-performance deep learning library. In H. Wallach, H. Larochelle, A. Beygelzimer, F. Alché-Buc, E. Fox, and R. Garnett, editors, *NeurIPS*, pages 8024–8035. Curran Associates, Inc., 2019.
- [31] E. Perez, F. Strub, H. De Vries, V. Dumoulin, and A. Courville. Film: Visual reasoning with a general conditioning layer. In *Proceedings of the AAAI Conference on Artificial Intelligence*, 2018.
- [32] S.-A. Rebuffi, H. Bilen, and A. Vedaldi. Learning multiple visual domains with residual adapters. In *NeurIPS*, 2017.
- [33] S.-A. Rebuffi, H. Bilen, and A. Vedaldi. Efficient parametrization of multi-domain deep neural networks. In *CVPR*, pages 8119–8127, 2018.
- [34] M. Ren, E. Triantafillou, S. Ravi, J. Snell, K. Swersky, J. B. Tenenbaum, H. Larochelle, and R. S. Zemel. Meta-learning for semi-supervised few-shot classification. In *ICLR*, 2018.
- [35] J. Requeima, J. Gordon, J. Bronskill, S. Nowozin, and R. E. Turner. Fast and flexible multi-task classification using conditional neural adaptive processes. In *NeurIPS*, 2019.
- [36] O. Russakovsky, J. Deng, H. Su, J. Krause, S. Satheesh, S. Ma, Z. Huang, A. Karpathy, A. Khosla, M. Bernstein, et al. Imagenet large scale visual recognition challenge. *IJCV*, 115(3):211–252, 2015.
- [37] A. A. Rusu, D. Rao, J. Sygnowski, O. Vinyals, R. Pascanu, S. Osindero, and R. Hadsell. Meta-learning with latent embedding optimization. In *ICLR*, 2020.

- [38] T. Saikia, T. Brox, and C. Schmid. Optimized generic feature learning for few-shot classification across domains. *arXiv preprint arXiv:2001.07926*, 2020.
- [39] J. Snell, K. Swersky, and R. S. Zemel. Prototypical networks for few-shot learning. In *NeurIPS*, 2017.
- [40] F. Sung, Y. Yang, L. Zhang, T. Xiang, P. H. Torr, and T. M. Hospedales. Learning to compare: Relation network for few-shot learning. In *CVPR*, pages 1199–1208, 2018.
- [41] Y. Tian, Y. Wang, D. Krishnan, J. B. Tenenbaum, and P. Isola. Rethinking few-shot image classification: a good embedding is all you need? In *ECCV*, 2020.
- [42] E. Triantafillou, H. Larochelle, R. Zemel, and V. Dumoulin. Learning a universal template for few-shot dataset generalization. In *ICML*, 2021.
- [43] E. Triantafillou, T. Zhu, V. Dumoulin, P. Lamblin, U. Evci, K. Xu, R. Goroshin, C. Gelada, K. Swersky, P.-A. Manzagol, et al. Meta-dataset: A dataset of datasets for learning to learn from few examples. In *ICLR*, 2020.
- [44] O. Vinyals, C. Blundell, T. Lillicrap, K. Kavukcuoglu, and D. Wierstra. Matching networks for one shot learning. In *NeurIPS*, 2016.
- [45] C. Wah, S. Branson, P. Welinder, P. Perona, and S. Belongie. The caltech-ucsd birds-200-2011 dataset. *California Institute of Technology*, 2011.
- [46] Y. Wang, Q. Yao, J. T. Kwok, and L. M. Ni. Generalizing from a few examples: A survey on few-shot learning. *ACM Computing Surveys (CSUR)*, 53(3):1–34, 2020.
- [47] M. D. Zeiler. Adadelta: an adaptive learning rate method. *arXiv preprint arXiv:1212.5701*, 2012.

A Dataset

Meta-Dataset [43] is a few-shot classification benchmark that initially consists of ten datasets: ILSVRC_2012 [36] (ImageNet), Omniglot [14], FGVC-Aircraft [25] (Aircraft), CUB-200-2011 [45] (Birds), Describable Textures [8] (DTD), QuickDraw [15], FGVCx Fungi [4] (Fungi), VGG Flower [28] (Flower), Traffic Signs [16] and MSCOCO [23] then further expands with MNIST [20], CIFAR-10 [10] and CIFAR-100 [10]. We follow the standard procedure and use the first eight datasets for meta-training, in which each dataset is further divided into train, validation and test set with disjoint classes. While the evaluation within these datasets is used to measure the generalization ability in the seen domains, the remaining five datasets are reserved as unseen domains in meta-test for measuring the cross-domain generalization ability. As in [42], we evaluate our method on 600 randomly sampled tasks for each dataset with varying number of ways and shots, and report average accuracy and 95% confidence score in all experiments.

B Implementation details

In all experiments we build our method on ResNet-18 [10] backbone for both single-domain and multi-domain networks.

B.1 Implementation details of representation learning

We follow the training protocol in [2]. We first train one ResNet-18 model for each training dataset and then we train a multi-domain learning network by URL [2].

Single domain learning. We train one ResNet-18 model for each training dataset. For optimization, we follow the training protocol in [10, 2]. Specifically, we use SGD optimizer and cosine annealing for all experiments with a momentum of 0.9 and a weight decay of 7×10^{-4} . The learning rate, batch size, annealing frequency, maximum number of iterations are shown in Table 5. To regularize training, we also use the exact same data augmentations as in [10, 2], *e.g.* random crops and random color augmentations.

Dataset	learning rate	batch size	annealing freq.	max. iter.
ImageNet	3×10^{-2}	64	48,000	480,000
Omniglot	3×10^{-2}	16	3000	50,000
Aircraft	3×10^{-2}	8	3000	50,000
Birds	3×10^{-2}	16	3000	50,000
Textures	3×10^{-2}	32	1500	50,000
Quick Draw	1×10^{-2}	64	48,000	480,000
Fungi	3×10^{-2}	32	15,000	480,000
VGG Flower	3×10^{-2}	8	1500	50,000

Table 5: Training hyper-parameters of single domain learning.

Multi-domain learning. In the multi-domain network, we share all the layers but the last classifier across the domains as in [2]. For multi-domain network optimization, we follow the same protocol in [2], use the same optimizer with a weight decay of 7×10^{-4} and a scheduler as single domain learning model for learning 240,000 iterations. The learning rate is 0.03 and the annealing frequency is 48,000. As in [2], the batch size for ImageNet is 64×7 and is 64 for the other 7 datasets.

We use the exactly same hyper-parameters as in [2] to obtain URL model. More specifically, we set the weight of CKA loss λ^f and the weight of distillation loss on predictions λ^p as 4 for ImageNet and 1 for other datasets, respectively. We also linearly anneal the λ^f and λ^p as in [2] and we refer readers to [2] for more details. For all experiments, early-stopping is performed based on cross-validation over the validations sets of 8 training datasets as in [2].

B.2 Implementation details of model adaptation

Predicting r_α . In case of modulating α with the auxiliary network, we follow the auxiliary training protocols in [2]. We train for 10K episodes to optimize the task encoder using Adam with a learning rate of 1×10^{-5} on eight training domains in meta-train. We validate every 5K iterations to save the best model for test.

Attaching and learning adapters. For the optimization of the adaptation parameters α which is attached directly and learned on support set and the pre-classifier adaptation ϑ , we follow the optimization strategy in [2], initialize ϑ as an identity matrix and optimize both α and ϑ for 40 iterations using Adadelta [2] as optimizer. The learning rate of ϑ is 0.1 for first eight datasets and 1 for the last five datasets as in [2] and we set the learning rate of α as half of the learning rate of ϑ , *i.e.* 0.05 for the first eight datasets and 0.5 for the last five datasets. Note that, we learn α and ϑ on a per-task basis using the task’s support set during meta-test. That is, α and ϑ are not re-used across the test tasks drawn from \mathcal{D}_t .

C More results

C.1 Detailed results of model adaptation methods

In the Table 6, we report the Mean accuracy, 95% confidence interval of each dataset for the comparison of different r_α choices. The first eight datasets are seen during training and the last five datasets are unseen and used for test only.

Test Dataset	classifier	Aux-Net or Ad	serial or parallel	M or CW	ϑ	#params	ImageNet	Omniglot	Aircraft	Birds	Textures	Quick Draw	Fungi	VGG Flower	Traffic Sign	MSCOCO	MNIST	CIFAR-10	CIFAR-100
NCC	NCC	-	-	-	\times	-	57.0 ± 1.1	94.4 ± 0.4	88.0 ± 0.5	80.3 ± 0.7	74.6 ± 0.7	81.8 ± 0.6	66.2 ± 0.9	91.5 ± 0.5	49.8 ± 1.1	54.1 ± 1.0	91.1 ± 0.4	70.6 ± 0.7	59.1 ± 1.0
MD	MD	-	-	-	\times	-	53.9 ± 1.0	93.8 ± 0.5	87.6 ± 0.5	78.3 ± 0.7	73.7 ± 0.7	80.9 ± 0.7	57.7 ± 0.9	89.7 ± 0.6	62.2 ± 1.1	48.5 ± 1.0	95.1 ± 0.4	68.9 ± 0.8	60.0 ± 0.9
LR	LR	-	-	-	\times	-	56.0 ± 1.1	93.7 ± 0.5	88.3 ± 0.5	79.7 ± 0.8	74.7 ± 0.7	80.0 ± 0.7	62.1 ± 0.8	91.1 ± 0.5	59.7 ± 1.1	54.2 ± 1.1	93.5 ± 0.2	73.1 ± 0.8	60.1 ± 1.1
SVM	SVM	-	-	-	\times	-	54.5 ± 1.1	94.3 ± 0.5	87.7 ± 0.5	78.1 ± 0.8	73.8 ± 0.8	80.0 ± 0.6	58.5 ± 0.9	91.4 ± 0.6	65.7 ± 1.2	50.5 ± 1.0	95.4 ± 0.2	72.0 ± 0.8	60.3 ± 1.1
Finetune	NCC	-	-	-	\times	-	55.9 ± 1.2	94.0 ± 0.5	87.3 ± 0.5	78.8 ± 0.9	76.8 ± 0.9	75.3 ± 0.9	57.6 ± 1.1	91.5 ± 0.6	86.1 ± 0.9	53.1 ± 1.0	96.8 ± 0.4	80.9 ± 0.8	65.9 ± 1.1
FILM-S	NCC	Aux-Net	serial	CW	\times	-	54.6 ± 1.1	93.5 ± 0.5	86.6 ± 0.5	78.6 ± 0.8	71.5 ± 0.7	79.3 ± 0.6	66.0 ± 0.9	87.6 ± 0.6	43.3 ± 0.9	49.1 ± 1.0	87.9 ± 0.5	62.8 ± 0.8	51.5 ± 1.0
FILM-R	NCC	Aux-Net	residual	CW	\times	-	56.1 ± 1.1	94.2 ± 0.4	88.4 ± 0.5	80.6 ± 0.7	74.9 ± 0.6	82.0 ± 0.6	66.4 ± 0.9	91.6 ± 0.5	48.5 ± 1.0	53.5 ± 1.0	90.8 ± 0.5	70.2 ± 0.8	59.7 ± 1.0
FILM-S	MD	Aux-Net	serial	CW	\times	-	55.1 ± 1.1	93.8 ± 0.5	86.8 ± 0.5	77.4 ± 0.8	73.2 ± 0.8	79.9 ± 0.7	57.4 ± 0.9	88.1 ± 0.7	58.4 ± 1.1	50.1 ± 1.1	92.7 ± 0.5	66.5 ± 0.8	55.7 ± 1.1
FILM-R	MD	Aux-Net	residual	CW	\times	-	54.8 ± 1.1	93.8 ± 0.5	87.4 ± 0.5	78.2 ± 0.7	73.4 ± 0.7	81.1 ± 0.7	58.8 ± 0.9	90.1 ± 0.5	63.6 ± 1.2	48.5 ± 1.1	94.8 ± 0.4	69.6 ± 0.8	60.6 ± 0.9
Ad-S-CW	NCC	Ad	serial	CW	✓	0.06	56.8 ± 1.1	94.8 ± 0.4	89.3 ± 0.5	80.7 ± 0.7	74.5 ± 0.7	81.6 ± 0.6	65.8 ± 0.9	91.3 ± 0.5	73.9 ± 1.1	53.6 ± 1.1	95.7 ± 0.4	78.4 ± 0.7	64.3 ± 1.0
Ad-R-CW (Ours)	NCC	Ad	residual	CW	✓	1.57%	57.6 ± 1.1	94.7 ± 0.4	89.0 ± 0.4	81.2 ± 0.8	75.2 ± 0.7	81.5 ± 0.6	65.4 ± 0.8	91.8 ± 0.5	79.2 ± 1.1	54.7 ± 1.1	96.4 ± 0.4	79.5 ± 0.8	67.4 ± 1.0
Ad-S-M	NCC	Ad	serial	M	✓	12.50%	56.2 ± 1.1	94.4 ± 0.4	89.1 ± 0.5	80.6 ± 0.7	75.8 ± 0.7	81.6 ± 0.6	67.1 ± 0.9	92.1 ± 0.4	67.6 ± 1.2	54.8 ± 1.1	95.9 ± 0.4	78.9 ± 0.7	66.6 ± 1.1
Ad-R-M (Ours)	NCC	Ad	residual	M	✓	10.93%	57.3 ± 1.1	94.9 ± 0.4	88.9 ± 0.5	81.0 ± 0.7	76.7 ± 0.7	80.6 ± 0.6	65.4 ± 0.9	91.4 ± 0.5	82.6 ± 1.0	55.0 ± 1.1	96.6 ± 0.4	82.1 ± 0.7	66.4 ± 1.1
Ad-R-CW-PA	NCC	Ad	serial	CW	✓	3.91%	58.6 ± 1.1	94.5 ± 0.4	90.0 ± 0.4	80.5 ± 0.8	77.6 ± 0.7	81.9 ± 0.6	67.0 ± 0.9	92.2 ± 0.5	80.2 ± 0.9	57.2 ± 1.0	96.1 ± 0.4	81.5 ± 0.8	71.4 ± 0.9
Ad-R-M-PA (Ours)	NCC	Ad	residual	M	✓	13.27%	59.5 ± 1.2	94.9 ± 0.4	89.9 ± 0.4	81.1 ± 0.8	77.5 ± 0.7	81.7 ± 0.6	66.3 ± 0.9	92.2 ± 0.5	82.8 ± 1.0	57.6 ± 1.0	96.7 ± 0.4	82.9 ± 0.7	70.4 ± 1.0

Table 6: Comparisons to methods that learn classifiers and model adaptation methods during meta-test stage based on URL model. NCC, MD, LR, SVM denote nearest centroid classifier, Mahalanobis distance, logistic regression, support vector machines respectively. ‘Aux-Net or Ad’ indicates using Auxiliary Network to predict α or attaching adapter α directly. ‘M or CW’ means using matrix multiplication or channel-wise scaling adapters. ‘S’ and ‘R’ denote serial adapter and residual adapter, respectively. ‘ ϑ ’ indicates using the pre-classifier adaptation. Mean accuracy, 95% confidence interval are reported. The first eight datasets are seen during training and the last five datasets are unseen and used for test only.

C.2 Detailed results of varying-way 5-shot and 5-way-1-shot

Detailed results of Varying-Way Five-Shot and Five-Way One-Shot scenarios are depicted in Table 7. In the table, we report the Mean accuracy, 95% confidence interval of each dataset. The first eight datasets are seen during training and the last five datasets are unseen and used for test only.

Test Dataset	Varying-Way Five-Shot					Five-Way One-Shot				
	Simple CNAPS [□]	SUR [□]	URT [□]	URL [□]	Ours	Simple CNAPS [□]	SUR [□]	URT [□]	URL [□]	Ours
ImageNet	47.2 \pm 1.0	46.7 \pm 1.0	48.6 \pm 1.0	49.4 \pm 1.0	48.3 \pm 1.0	42.6 \pm 0.9	40.7 \pm 1.0	47.4 \pm 1.0	49.6 \pm 1.1	48.0 \pm 1.0
Omniglot	95.1 \pm 0.3	95.8 \pm 0.3	96.0 \pm 0.3	96.0 \pm 0.3	96.8 \pm 0.3	93.1 \pm 0.5	93.0 \pm 0.7	95.6 \pm 0.5	95.8 \pm 0.5	96.3 \pm 0.4
Aircraft	74.6 \pm 0.6	82.1 \pm 0.6	81.2 \pm 0.6	84.8 \pm 0.5	85.5 \pm 0.5	65.8 \pm 0.9	67.1 \pm 1.4	77.9 \pm 0.9	79.6 \pm 0.9	79.6 \pm 0.9
Birds	69.6 \pm 0.7	62.8 \pm 0.9	71.2 \pm 0.7	76.0 \pm 0.6	76.6 \pm 0.6	67.9 \pm 0.9	59.2 \pm 1.0	70.9 \pm 0.9	74.9 \pm 0.9	74.5 \pm 0.9
Textures	57.5 \pm 0.7	60.2 \pm 0.7	65.2 \pm 0.7	69.1 \pm 0.6	68.3 \pm 0.7	42.2 \pm 0.8	42.5 \pm 0.8	49.4 \pm 0.9	53.6 \pm 0.9	54.5 \pm 0.9
Quick Draw	70.9 \pm 0.6	79.0 \pm 0.5	79.2 \pm 0.5	78.2 \pm 0.5	77.9 \pm 0.6	70.5 \pm 0.9	79.8 \pm 0.9	79.6 \pm 0.9	79.0 \pm 0.8	79.3 \pm 0.9
Fungi	50.3 \pm 1.0	66.5 \pm 0.8	66.9 \pm 0.9	70.0 \pm 0.8	70.4 \pm 0.8	58.3 \pm 1.1	64.8 \pm 1.1	71.0 \pm 1.0	75.2 \pm 1.0	75.3 \pm 1.0
VGG Flower	86.5 \pm 0.4	76.9 \pm 0.6	82.4 \pm 0.5	89.3 \pm 0.4	89.5 \pm 0.4	79.9 \pm 0.7	65.0 \pm 1.0	72.7 \pm 0.0	79.9 \pm 0.8	80.3 \pm 0.8
Traffic Sign	55.2 \pm 0.8	44.9 \pm 0.9	45.1 \pm 0.9	57.5 \pm 0.8	72.3 \pm 0.6	55.3 \pm 0.9	44.6 \pm 0.9	52.7 \pm 0.9	57.9 \pm 0.9	57.2 \pm 1.0
MSCOCO	49.2 \pm 0.8	48.1 \pm 0.9	52.3 \pm 0.9	56.1 \pm 0.8	56.0 \pm 0.8	48.8 \pm 0.9	47.8 \pm 1.1	56.9 \pm 1.1	59.2 \pm 1.0	59.9 \pm 1.0
MNIST	88.9 \pm 0.4	90.1 \pm 0.4	86.5 \pm 0.5	89.7 \pm 0.4	92.5 \pm 0.4	80.1 \pm 0.9	77.1 \pm 0.9	75.6 \pm 0.9	78.7 \pm 0.9	80.1 \pm 0.9
CIFAR-10	66.1 \pm 0.7	50.3 \pm 1.0	61.4 \pm 0.7	66.0 \pm 0.7	72.0 \pm 0.7	50.3 \pm 0.9	35.8 \pm 0.8	47.3 \pm 0.9	54.7 \pm 0.9	55.8 \pm 0.9
CIFAR-100	53.8 \pm 0.9	46.4 \pm 0.9	52.5 \pm 0.9	57.0 \pm 0.9	64.1 \pm 0.8	53.8 \pm 0.9	42.9 \pm 1.0	54.9 \pm 1.1	61.8 \pm 1.0	63.7 \pm 1.0
Average Seen	69.0	71.2	73.8	76.6	76.7	65.0	64.0	70.6	73.4	73.5
Average Unseen	62.6	56.0	59.6	65.2	71.4	57.7	49.6	57.5	62.4	63.4
Average All	66.5	65.4	68.3	72.2	74.6	62.2	58.5	65.5	69.2	69.6
Average Rank	4.1	3.9	3.4	2.1	1.5	3.8	4.5	3.3	1.7	1.7

Table 7: Results of Varying-Way Five-Shot and Five-Way One-Shot scenarios. Mean accuracy, 95% confidence interval are reported.

C.3 Detailed results of ablation study.

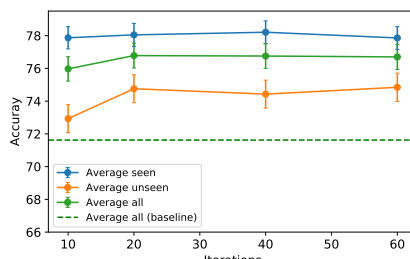


Figure 5: Sensitivity of performance to number of iterations based on MDL model.

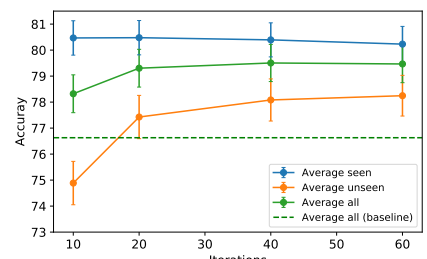


Figure 6: Sensitivity of performance to number of iterations based on URL model.

Sensitivity analysis for number of iterations. In our method, we optimize the attached parameters (α, ϑ) with 40 iterations. Figure 5 and Figure 6 report the results with 10, 20, 40, 60 iterations and indicates that our method (solid green) converges to a stable solution after 20 iterations and achieves better average performance on all domains than the baseline URL (dash green). The mean accuracy with 95% confidence interval are reported in Tables 8 and 9.

Influence of α and ϑ . We evaluate different components of our methods and report the results in Table 10. The results show that both residual adapters α and the linear transformation ϑ help adapt features to unseen classes while residual adapters significantly improve the performance on unseen domains. The best results are achieved by using both α and ϑ .

Test Dataset	ImageNet	Omniglot	Aircraft	Birds	Textures	Quick Draw	Fungi	VGG Flower	Traffic Sign	MSCOCO	MNIST	CIFAR-10	CIFAR-100
10 iterations	55.5 ± 1.1	93.9 ± 0.5	86.4 ± 0.5	78.6 ± 0.7	73.3 ± 0.7	81.9 ± 0.6	63.1 ± 0.9	90.3 ± 0.5	77.6 ± 1.0	50.6 ± 1.1	96.9 ± 0.3	77.0 ± 0.8	62.6 ± 1.1
20 iterations	56.2 ± 1.1	94.7 ± 0.4	86.3 ± 0.5	78.3 ± 0.8	73.9 ± 0.7	81.6 ± 0.6	63.4 ± 0.9	90.1 ± 0.6	79.4 ± 1.0	52.8 ± 1.1	97.2 ± 0.3	78.6 ± 0.8	65.9 ± 1.1
40 iterations	55.6 ± 1.0	94.3 ± 0.4	86.7 ± 0.5	79.4 ± 0.8	73.2 ± 0.8	81.7 ± 0.6	64.0 ± 0.9	90.9 ± 0.5	81.1 ± 0.9	51.4 ± 1.1	96.9 ± 0.3	78.5 ± 0.8	64.3 ± 1.1
60 iterations	55.9 ± 1.1	95.1 ± 0.4	85.9 ± 0.6	77.5 ± 0.8	74.7 ± 0.7	80.9 ± 0.6	62.1 ± 0.9	90.7 ± 0.6	82.2 ± 0.9	52.2 ± 1.1	97.0 ± 0.4	78.4 ± 0.8	64.4 ± 1.1

Table 8: Sensitivity of performance to number of iterations based on MDL model.

Test Dataset	ImageNet	Omniglot	Aircraft	Birds	Textures	Quick Draw	Fungi	VGG Flower	Traffic Sign	MSCOCO	MNIST	CIFAR-10	CIFAR-100
10 iterations	58.4 ± 1.1	94.8 ± 0.4	89.9 ± 0.4	81.3 ± 0.7	76.6 ± 0.7	81.8 ± 0.6	68.4 ± 0.9	92.5 ± 0.5	76.5 ± 1.1	55.6 ± 1.1	96.4 ± 0.4	79.0 ± 0.7	66.9 ± 1.0
20 iterations	58.2 ± 1.1	94.8 ± 0.4	89.9 ± 0.4	81.1 ± 0.7	77.5 ± 0.8	81.9 ± 0.6	68.0 ± 0.9	92.4 ± 0.5	81.8 ± 1.0	57.8 ± 1.1	96.7 ± 0.4	81.7 ± 0.8	69.1 ± 0.9
40 iterations	59.5 ± 1.0	94.9 ± 0.4	89.9 ± 0.4	81.1 ± 0.8	77.5 ± 0.7	81.7 ± 0.6	66.3 ± 0.9	92.2 ± 0.5	82.8 ± 1.0	57.6 ± 1.0	96.7 ± 0.4	82.9 ± 0.7	70.4 ± 1.0
60 iterations	58.7 ± 1.1	94.9 ± 0.4	89.5 ± 0.5	80.8 ± 0.7	77.4 ± 0.8	81.8 ± 0.6	66.2 ± 0.9	92.5 ± 0.5	83.7 ± 0.9	56.9 ± 1.0	96.6 ± 0.3	82.0 ± 0.8	72.0 ± 0.9

Table 9: Sensitivity of performance to number of iterations based on URL model.

Test Dataset	ImageNet	Omniglot	Aircraft	Birds	Textures	Quick Draw	Fungi	VGG Flower	Traffic Sign	MSCOCO	MNIST	CIFAR-10	CIFAR-100
Ours w/o α & ϑ	57.0 ± 1.1	94.4 ± 0.4	88.0 ± 0.5	80.3 ± 0.7	74.6 ± 0.7	81.8 ± 0.6	66.2 ± 0.9	91.5 ± 0.5	49.8 ± 1.1	54.1 ± 1.0	91.1 ± 0.4	70.6 ± 0.7	59.1 ± 1.0
Ours w/o ϑ	57.3 ± 1.1	94.9 ± 0.4	88.9 ± 0.5	81.0 ± 0.7	76.7 ± 0.7	80.6 ± 0.6	65.4 ± 0.9	91.4 ± 0.5	82.6 ± 1.0	55.0 ± 1.1	96.6 ± 0.4	82.1 ± 0.7	66.4 ± 1.1
Ours w/o α	58.8 ± 1.1	94.5 ± 0.4	89.4 ± 0.4	80.7 ± 0.8	77.2 ± 0.7	82.5 ± 0.6	68.1 ± 0.9	92.0 ± 0.5	63.3 ± 1.2	57.3 ± 1.0	94.7 ± 0.4	74.2 ± 0.8	63.6 ± 1.0
Ours	59.5 ± 1.0	94.9 ± 0.4	89.9 ± 0.4	81.1 ± 0.8	77.5 ± 0.7	81.7 ± 0.6	66.3 ± 0.9	92.2 ± 0.5	82.8 ± 1.0	57.6 ± 1.0	96.7 ± 0.4	82.9 ± 0.7	70.4 ± 1.0

Table 10: Effect of each component. ‘Ours w/o α & ϑ ’ means we remove both residual adapters α and the pre-classifier adaptation layer ϑ in our method.

Initialization analysis for adapters. Here, we investigate using different initialization strategies for adapters: i) Identity initialization: in this work we initialize each residual adapter as an identity matrix scaled by a scalar δ and we set $\delta = 1e-4$; ii) randomly initialization: alternatively, we can randomly initialize each residual adapter. The results of different initialization are summarized in Fig. 7. We can see that our methods with different initialization strategies obtain similar results, which indicates that our method works also with randomly initialization and again verifies the stability of our method. Detailed results of each datasets are shown in Table 11.

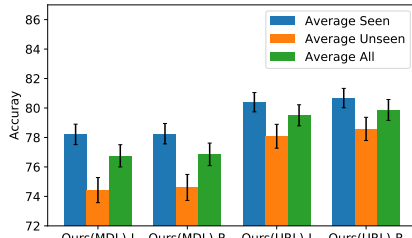


Figure 7: Initialization analysis for adapters. ‘Ours(MDL)-I’ indicates identity initialization and ‘-R’ is randomly initialization.

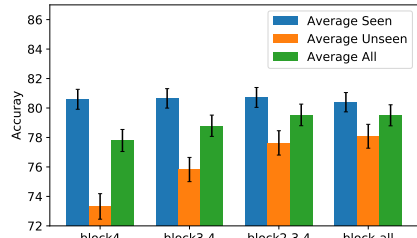


Figure 8: Block (layer) analysis for adapters.

Test Dataset	ImageNet	Omniglot	Aircraft	Birds	Textures	Quick Draw	Fungi	VGG Flower	Traffic Sign	MSCOCO	MNIST	CIFAR-10	CIFAR-100
Ours(ImageNet)-I	59.5 ± 1.1	78.2 ± 1.2	72.2 ± 1.0	74.9 ± 0.9	77.3 ± 0.7	67.6 ± 0.9	44.7 ± 1.0	90.9 ± 0.6	82.5 ± 0.3	59.0 ± 1.0	93.9 ± 0.6	82.1 ± 0.7	70.7 ± 0.9
Ours(ImageNet)-R	58.2 ± 1.0	78.4 ± 1.2	71.1 ± 1.1	74.4 ± 1.0	77.1 ± 0.7	67.2 ± 1.0	45.9 ± 1.0	90.7 ± 0.6	81.9 ± 1.0	57.7 ± 1.1	94.1 ± 0.5	81.9 ± 0.7	70.5 ± 0.9
Ours(MDL)-I	55.6 ± 1.0	94.3 ± 0.4	86.7 ± 0.5	79.4 ± 0.8	73.2 ± 0.8	81.7 ± 0.6	64.0 ± 0.9	90.9 ± 0.5	81.1 ± 0.9	51.4 ± 1.1	96.9 ± 0.3	78.5 ± 0.8	64.3 ± 1.1
Ours(MDL)-R	56.0 ± 1.1	94.1 ± 0.4	87.1 ± 0.5	79.7 ± 0.8	74.0 ± 0.7	82.0 ± 0.6	62.6 ± 0.9	90.6 ± 0.6	80.9 ± 0.9	51.7 ± 1.1	96.9 ± 0.4	77.7 ± 0.9	65.8 ± 1.1
Ours(URL)-I	59.5 ± 1.0	94.9 ± 0.4	89.9 ± 0.4	81.1 ± 0.8	77.5 ± 0.7	81.7 ± 0.6	66.3 ± 0.9	92.2 ± 0.5	82.8 ± 1.0	57.6 ± 1.0	96.7 ± 0.4	82.9 ± 0.7	70.4 ± 1.0
Ours(URL)-R	58.8 ± 1.1	94.9 ± 0.4	90.5 ± 0.4	81.8 ± 0.6	77.7 ± 0.7	82.3 ± 0.6	66.8 ± 0.9	92.6 ± 0.5	83.7 ± 0.8	57.7 ± 1.1	96.9 ± 0.4	82.5 ± 0.7	72.0 ± 0.9

Table 11: Initialization analysis of adapters. ‘Ours(URL)-I’ indicates our method using URL as the pretrained model and initializing residual adapters as identity matrix (scaled by $\delta = 0.0001$) while ‘Ours(URL)-R’ means our method initialize residual adapters randomly.

Layer analysis for adapters. Here we investigate whether it is sufficient to attach the adapters only to the later layers. We evaluate this on ResNet18 which is composed of four blocks and attach the adapters to only later blocks (block4, block3,4, block2,3,4 and block-all). Figure 8 shows that applying our adapters to only the last block (block4) obtains around 78% average accuracy on all domains which outperforms the URL. With attaching residual adapters to more layers, the performance on unseen domains is improved significantly while the one on seen domains remains stable. The mean accuracy with 95% confidence interval for layer analysis are shown in Table 12.

Test Dataset	ImageNet	Omniglot	Aircraft	Birds	Textures	Quick Draw	Fungi	VGG Flower	Traffic Sign	MSCOCO	MNIST	CIFAR-10	CIFAR-100
Ours (block4)	59.0 ± 1.1	95.0 ± 0.4	90.0 ± 0.4	80.6 ± 0.8	77.8 ± 0.7	82.3 ± 0.6	68.2 ± 0.9	91.8 ± 0.6	70.6 ± 1.1	57.1 ± 1.1	95.9 ± 0.4	77.2 ± 0.8	65.9 ± 1.0
Ours (block3,4)	60.4 ± 1.1	94.7 ± 0.4	90.0 ± 0.5	80.4 ± 0.7	77.8 ± 0.7	82.2 ± 0.6	67.2 ± 0.8	92.5 ± 0.5	77.2 ± 1.0	57.9 ± 1.0	96.7 ± 0.3	78.8 ± 0.9	68.6 ± 0.9
Ours (block2,3,4)	59.6 ± 1.1	94.9 ± 0.4	89.9 ± 0.5	81.0 ± 0.8	78.2 ± 0.7	82.4 ± 0.6	67.6 ± 0.9	92.3 ± 0.5	81.5 ± 1.0	57.9 ± 1.0	96.6 ± 0.4	81.5 ± 0.8	70.6 ± 1.0
Ours (block-all)	59.5 ± 1.0	94.9 ± 0.4	89.9 ± 0.4	81.1 ± 0.8	77.5 ± 0.7	81.7 ± 0.6	66.3 ± 0.9	92.2 ± 0.5	82.8 ± 1.0	57.6 ± 1.0	96.7 ± 0.4	82.9 ± 0.7	70.4 ± 1.0

Table 12: Block (layer) analysis for adapters based on URL model.

Decomposing residual adapters. Here we investigate whether one can reduce the number of parameters in the adapters while retaining its performance by using matrix decomposition. As in deep neural network, the adapters in earlier layers are relatively small, we then decompose the adapters in the last two blocks only where the adapter dimensionality goes up to 512×512 . Figure 9 shows that our method can achieve good performance with less parameters by decomposing large residual adapters, (e.g. when $N = 32$ where the number of additional parameters equal to around 4% vs 13%, the performance is still comparable to the original form of residual adapters, *i.e.* $N=0$). Results of each datasets in Table 13, also show that, by decomposing large residual adapters, the performance of our method is still comparable to the original form of residual adapters (*i.e.* Ours) with less parameters.

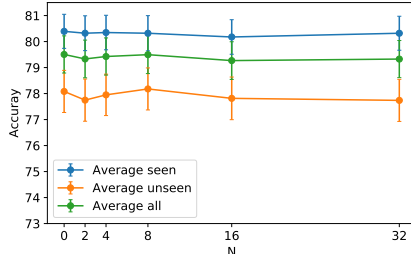


Figure 9: Decomposed residual adapters on block-3,4.

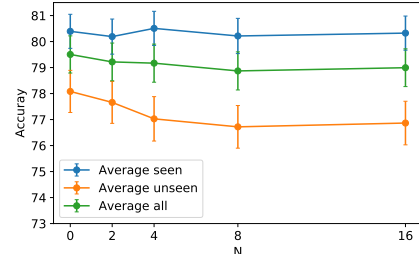


Figure 10: Decomposed residual adapters on all layers.

Test Dataset	ImageNet	Omniglot	Aircraft	Birds	Textures	Quick Draw	Fungi	VGG Flower	Traffic Sign	MSCOCO	MNIST	CIFAR-10	CIFAR-100
Ours	59.5 ± 1.0	94.9 ± 0.4	89.9 ± 0.4	81.1 ± 0.8	77.5 ± 0.7	81.7 ± 0.6	66.3 ± 0.9	92.2 ± 0.5	82.8 ± 1.0	57.6 ± 1.0	96.7 ± 0.4	82.9 ± 0.7	70.4 ± 1.0
Ours(N=2)	58.9 ± 1.1	95.2 ± 0.4	89.7 ± 0.5	80.9 ± 0.7	76.7 ± 0.7	81.4 ± 0.6	67.7 ± 0.9	92.2 ± 0.5	82.4 ± 1.0	57.1 ± 1.0	96.5 ± 0.4	82.4 ± 0.7	70.3 ± 1.0
Ours(N=4)	58.7 ± 1.1	94.9 ± 0.4	89.7 ± 0.5	80.3 ± 0.7	77.0 ± 0.7	82.5 ± 0.6	67.2 ± 0.9	92.5 ± 0.5	82.6 ± 1.0	57.5 ± 1.1	96.5 ± 0.4	82.5 ± 0.7	70.8 ± 0.9
Ours(N=8)	59.1 ± 1.1	95.0 ± 0.4	89.8 ± 0.5	80.2 ± 0.8	77.2 ± 0.7	82.1 ± 0.6	67.0 ± 0.9	92.2 ± 0.5	82.5 ± 1.0	57.2 ± 1.1	96.8 ± 0.4	82.6 ± 0.7	71.8 ± 0.9
Ours(N=16)	58.2 ± 1.1	94.7 ± 0.4	90.1 ± 0.4	80.3 ± 0.8	76.9 ± 0.7	81.7 ± 0.6	67.6 ± 0.9	92.0 ± 0.5	81.8 ± 1.0	58.1 ± 1.1	96.4 ± 0.4	81.8 ± 0.7	71.1 ± 0.9
Ours(N=32)	59.2 ± 1.1	94.8 ± 0.4	89.6 ± 0.5	80.0 ± 0.8	77.3 ± 0.6	82.4 ± 0.6	67.2 ± 0.9	92.1 ± 0.5	82.1 ± 1.0	57.1 ± 1.0	96.7 ± 0.3	81.6 ± 0.8	71.1 ± 0.9

Table 13: Results of using decomposed RA on layer3,4.

The similar conclusion can be drawn from results (shown in Fig. 10) of our method using decomposed residual adapters in all layers. When N increases, *i.e.*, smaller residual adapters, the average accuracy on all domains is still comparable to the original form of residual adapters (*i.e.* $N=0$) with less parameters though the average accuracy on unseen domains

drops slightly. From the results depicted in Table 14, we can see that when N increases, the performance of most domains are still comparable to the original form of residual adapters (*i.e.* Ours) while the performance on Traffic Sign drops slightly as the adapters in earlier layers are small and when N is larger the decomposed residual adapters might be too small to transform the features. In overall, our method can achieve good performance with less parameters by decomposing large residual adapters.

Test Dataset	ImageNet	Omniglot	Aircraft	Birds	Textures	Quick Draw	Fungi	VGG Flower	Traffic Sign	MSCOCO	MNIST	CIFAR-10	CIFAR-100
Ours	59.5 \pm 1.0	94.9 \pm 0.4	89.9 \pm 0.4	81.1 \pm 0.8	77.5 \pm 0.7	81.7 \pm 0.6	66.3 \pm 0.9	92.2 \pm 0.5	82.8 \pm 1.0	57.6 \pm 1.0	96.7 \pm 0.4	82.9 \pm 0.7	70.4 \pm 1.0
Ours(N=2)	58.1 \pm 1.1	94.8 \pm 0.4	89.7 \pm 0.5	80.2 \pm 0.8	76.9 \pm 0.7	82.1 \pm 0.6	67.8 \pm 0.9	92.0 \pm 0.6	82.5 \pm 0.9	56.9 \pm 1.1	96.7 \pm 0.3	82.0 \pm 0.8	70.3 \pm 1.0
Ours(N=4)	59.6 \pm 1.1	94.8 \pm 0.4	89.9 \pm 0.5	80.3 \pm 0.8	77.4 \pm 0.7	82.6 \pm 0.6	66.6 \pm 0.9	92.9 \pm 0.5	79.7 \pm 1.1	57.6 \pm 1.1	96.5 \pm 0.4	80.9 \pm 0.8	70.6 \pm 1.0
Ours(N=8)	58.2 \pm 1.1	94.6 \pm 0.4	89.6 \pm 0.5	81.2 \pm 0.8	76.6 \pm 0.7	82.7 \pm 0.6	66.5 \pm 0.9	92.3 \pm 0.5	78.1 \pm 1.1	57.3 \pm 1.0	96.3 \pm 0.3	81.0 \pm 0.8	70.9 \pm 0.9
Ours(N=16)	58.9 \pm 1.1	94.6 \pm 0.4	89.7 \pm 0.5	80.1 \pm 0.7	77.0 \pm 0.7	82.1 \pm 0.6	68.4 \pm 0.9	91.9 \pm 0.5	78.3 \pm 1.0	57.8 \pm 1.1	96.0 \pm 0.4	82.0 \pm 0.7	70.3 \pm 1.0

Table 14: Results of using decomposed RA on all layers.

C.4 Qualitative results

We qualitatively analyze our method and compare it to Simple CNAPS [2], SUR [10], URT [24], and URL [22] in Figs. 11 to 23 by illustrating the nearest neighbors in all test datasets given a query image as in [2]. It is clear that our method produces more correct neighbors than other methods. While other methods retrieves images with more similar colors, shapes and backgrounds, *e.g.* in Figs. 19, 20, 22 and 23, our method is able to retrieve semantically similar images. It again suggests that our method is able to quickly adapt the features for unseen few-shot tasks.



Figure 11: Qualitative comparison to Simple CNAPS [2], SUR [10], URT [24], and URL [22] in ImageNet. Green and red colors indicate correct and false predictions respectively.

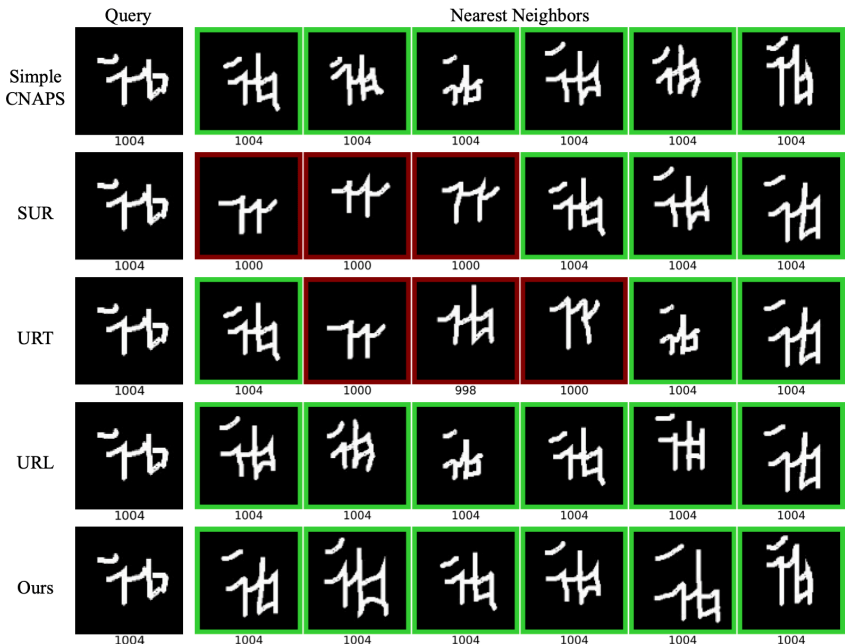


Figure 12: Qualitative comparison to Simple CNAPS [□], SUR [□], URT [□], and URL [□] in Omniglot. Green and red colors indicate correct and false predictions respectively.

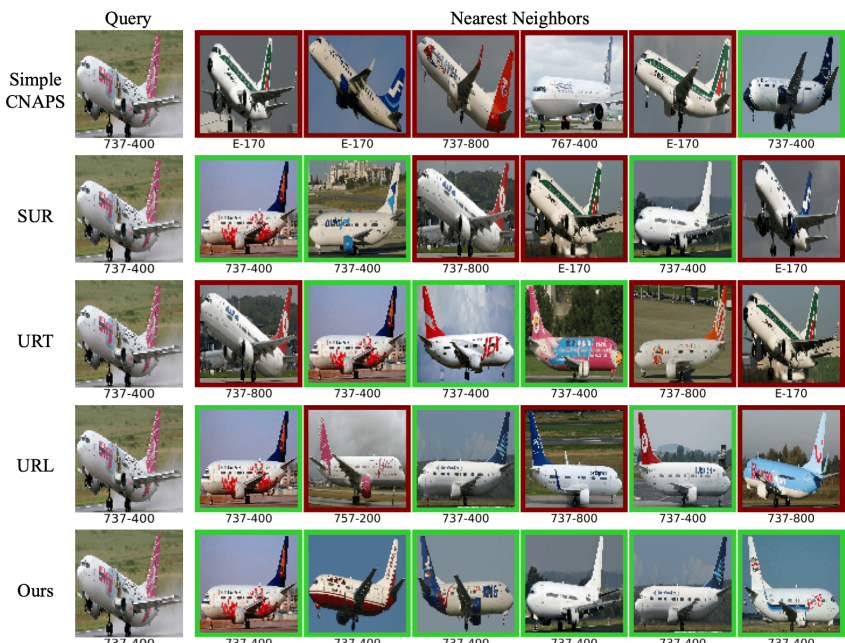
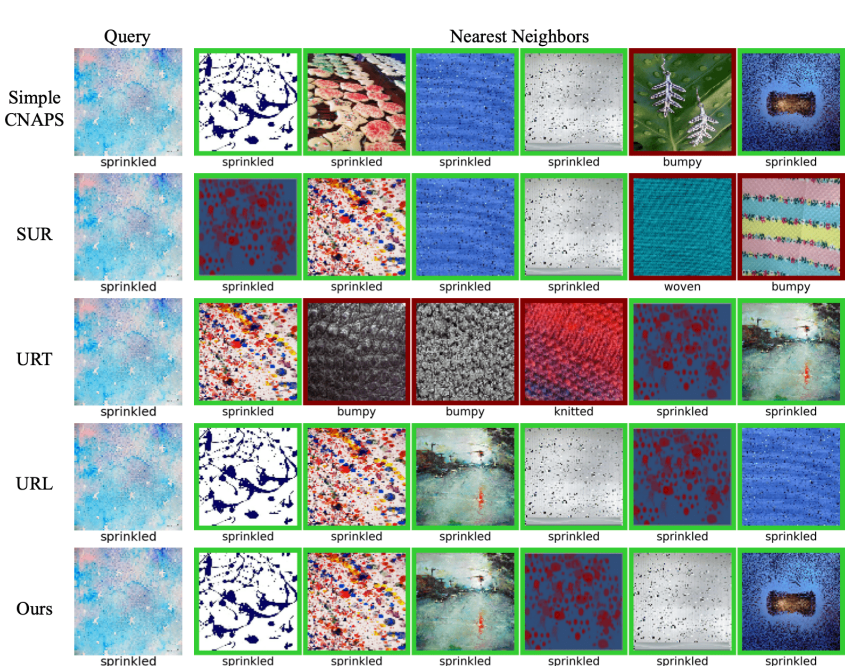
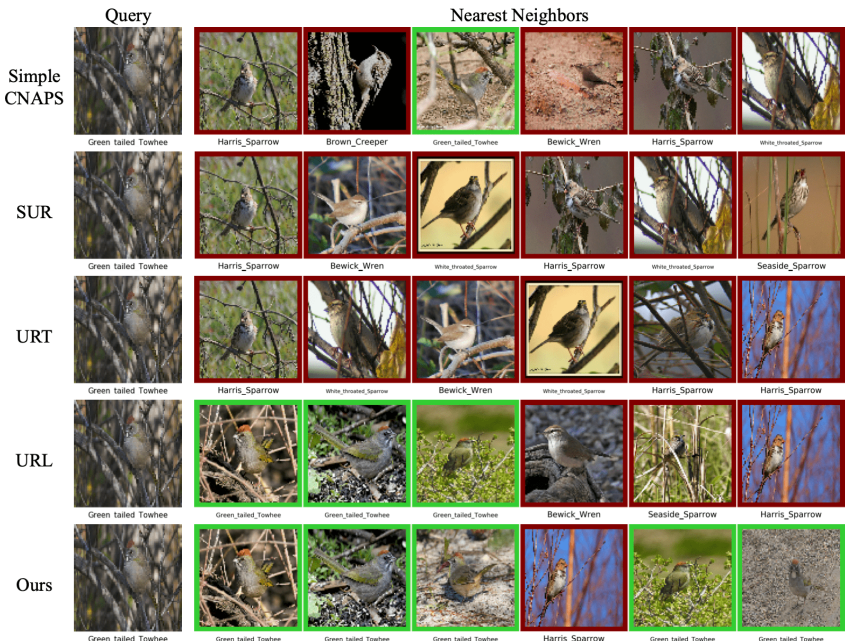


Figure 13: Qualitative comparison to Simple CNAPS [□], SUR [□], URT [□], and URL [□] in Aircraft. Green and red colors indicate correct and false predictions respectively.



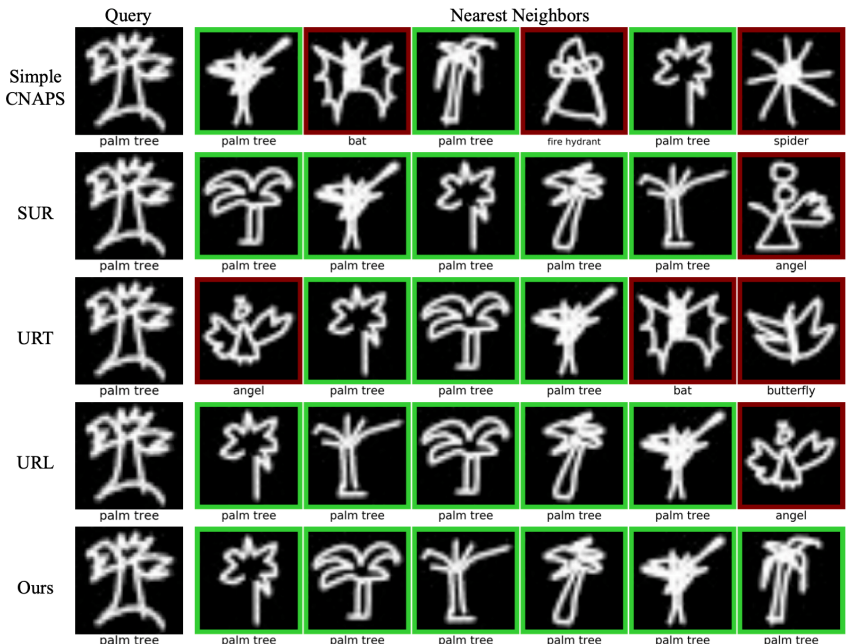


Figure 16: Qualitative comparison to Simple CNAPS [◻], SUR [◼], URT [◼], and URL [◼] in Quick Draw. Green and red colors indicate correct and false predictions respectively.



Figure 17: Qualitative comparison to Simple CNAPS [◻], SUR [◼], URT [◼], and URL [◼] in Fungi. Green and red colors indicate correct and false predictions respectively.



Figure 18: Qualitative comparison to Simple CNAPS [1], SUR [10], URT [24], and URL [27] in VGG Flower. Green and red colors indicate correct and false predictions respectively.



Figure 19: Qualitative comparison to Simple CNAPS [1], SUR [10], URT [24], and URL [27] in Traffic Sign. Green and red colors indicate correct and false predictions respectively.



Figure 20: Qualitative comparison to Simple CNAPS [◻], SUR [◻], URT [◻], and URL [◻] in MSCOCO. Green and red colors indicate correct and false predictions respectively.

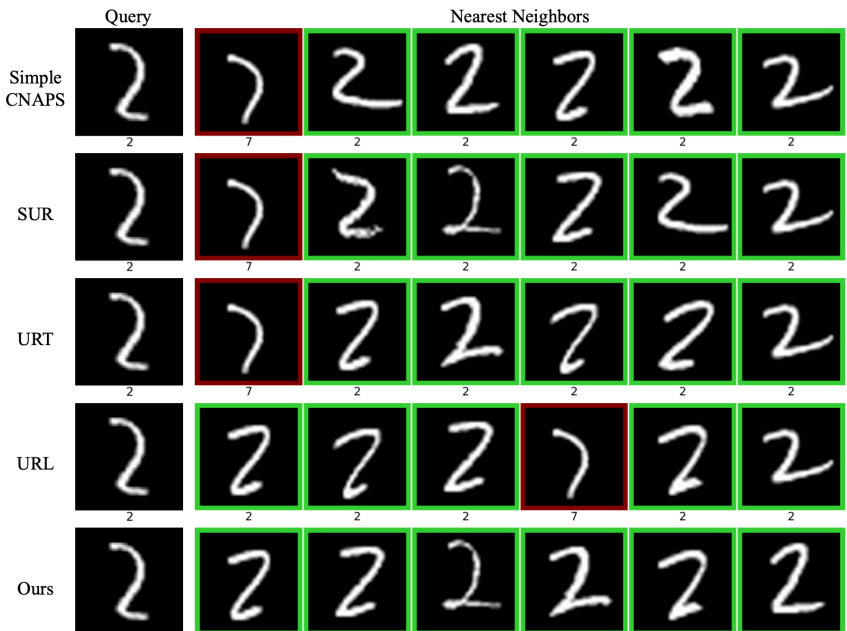


Figure 21: Qualitative comparison to Simple CNAPS [◻], SUR [◻], URT [◻], and URL [◻] in MNIST. Green and red colors indicate correct and false predictions respectively.

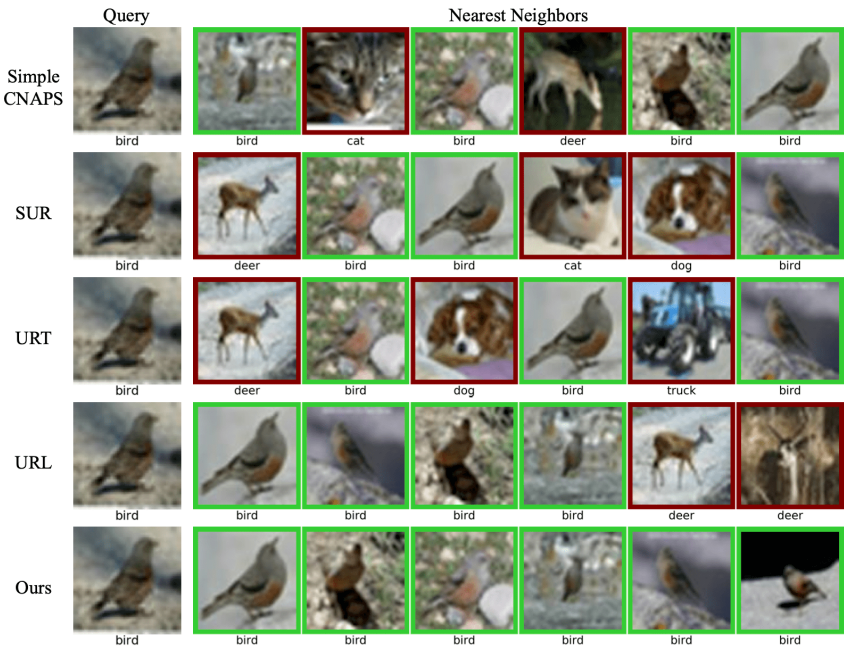


Figure 22: Qualitative comparison to Simple CNAPS [2], SUR [10], URT [24], and URL [27] in CIFAR-10. Green and red colors indicate correct and false predictions respectively.

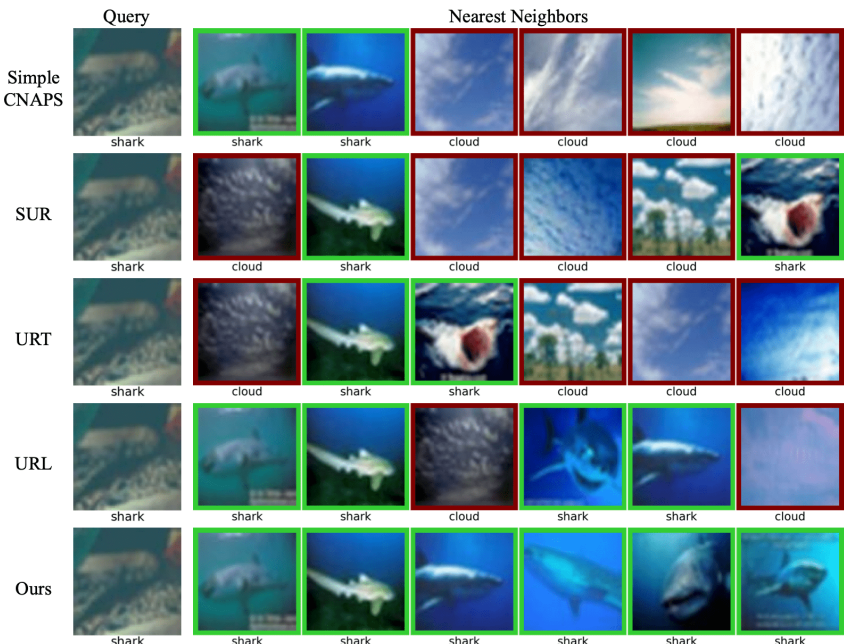


Figure 23: Qualitative comparison to Simple CNAPS [2], SUR [10], URT [24], and URL [27] in CIFAR-100. Green and red colors indicate correct and false predictions respectively.